Journal of
Synchrotron Radiation

ISSN 0909-0495

Received 26 March 2010
Accepted 18 June 2010

A confocal set-up for micro-XRF and XAFS experiments using diamond-anvil cells

Max Wilke,[a]* Karen Appel,[b] Laszlo Vincze,[c] Christian Schmidt,[a] Manuela Borchert[b,a,d] and Sakura Pascarelli[e]

[a]Helmholtzzentrum Potsdam Deutsches GeoForschungsZentrum (GFZ), Telegrafenberg, 14473 Potsdam, Germany, [b]Deutsches Elektronen-Synchrotron, Ein Forschungszentrum der Helmholtz-Gemeinschaft, Notkestrasse 85, 22607 Hamburg, Germany, [c]Department of Analytical Chemistry, Ghent University, Krijgslaan 281, 9000 Gent, Belgium, [d]Institut für Erd- und Umweltwissenschaften, Universität Potsdam, Karl-Liebknecht-Strasse 25, 14476 Potsdam-Golm, Germany, and [e]European Synchrotron Radiation Facility, BP 220, 38043 Grenoble Cedex, France.
E-mail: max@gfz-potsdam.de

A confocal set-up is presented that improves micro-XRF and XAFS experiments with high-pressure diamond-anvil cells (DACs). In this experiment a probing volume is defined by the focus of the incoming synchrotron radiation beam and that of a polycapillary X-ray half-lens with a very long working distance, which is placed in front of the fluorescence detector. This set-up enhances the quality of the fluorescence and XAFS spectra, and thus the sensitivity for detecting elements at low concentrations. It efficiently suppresses signal from outside the sample chamber, which stems from elastic and inelastic scattering of the incoming beam by the diamond anvils as well as from excitation of fluorescence from the body of the DAC.

Keywords: XRF; XAFS; high pressure; aqueous fluids.

1. Introduction

The combination of high-pressure devices and X-ray techniques based on synchrotron radiation has become a standard experimental set-up for studying materials at high pressure and temperature. A large number of these studies are performed using diamond-anvil cells (DACs) owing to the low absorption of hard X-rays by diamond and to the extreme pressure conditions that can be reached (*e.g.* Keppler & Frost, 2005; Boehler, 2005). While X-ray diffraction using these cells has been a standard technique for quite a long time, the application of X-ray fluorescence (XRF) analysis to quantify element concentrations of the sample in the DAC has only been applied lately (Schmidt & Rickers, 2003; Sanchez-Valle *et al.*, 2003). These and subsequent studies (Sanchez-Valle *et al.*, 2004; Schmidt *et al.*, 2006, 2007; Manning *et al.*, 2008; Borchert *et al.*, 2009) have shown that detection limits in the lower p.p.m. range can be reached for elements down to atomic number 22 (Ti). These high sensitivities have been achieved using an intense focused synchrotron radiation beam and/or modifications of the cells to optimize the signal-to-background ratio of the fluorescence signal. In this way it was even possible to obtain X-ray absorption spectra (XAFS) of dilute elements in melts and solutions at high pressure and temperature (*e.g.* Wilke *et al.*, 2006; Mayanovic *et al.*, 2007). A substantial contribution to the background of the fluorescence spectra stems from inelastic scattering of the incoming beam as it travels through the upstream diamond anvil. Acquisition of the XRF spectra with the detector at 90° to the incoming beam minimizes the inelastic scattering signal for linearly polarized synchrotron radiation because the scattering cross section along the E vector is zero (*e.g.* Haller & Knöchel, 1996; Schmidt & Rickers, 2003). However, a substantial amount of elastically and inelastically scattered radiation is recorded even in this configuration because the detector's solid angle is finite and not only signal along the E vector is recorded. Furthermore, the focused beam is blurred by a halo of scattered radiation produced in the diamond anvil, which deteriorates the spatial resolution of the set-up. This effect may limit the applicability of the technique for samples that are heterogeneous on the microscopic scale. A high spatial resolution is also important for DAC experiments at extreme pressures (up to 100 GPa), in which the total sample size is only in the region of 50 µm.

Here, we tested a confocal micro-XRF set-up to overcome these limitations. The confocal set-up is similar to the one proposed by Kanngiesser *et al.* (2003), Janssens *et al.* (2004) and Vincze *et al.* (2004). In these experiments a probing volume is defined by coinciding the focal spot of an additional X-ray optic in front of the detector with the focal spot of the incoming beam. This arrangement minimizes signal contributions from the space outside the focal spot of the beam and even allows acquisition of chemical information in three dimensions (*e.g.* Kanngiesser *et al.*, 2003; Janssens *et al.*, 2004;

Vincze *et al.*, 2004). While the normal confocal set-up is optimized for spatial resolution, a confocal set-up for a DAC has to find a trade-off between spatial resolution and the focal distance that is required by the DAC. In the set-up presented here, we used a glass polycapillary with a long focal distance as X-ray half-lens in front of the detector.

2. Experimental

2.1. Detector polycapillary

The polycapillary half-lens was designed to provide a focal spot of ~150–300 µm at a focal distance of 50 mm. It was optimized to work between 6 and 18 keV to cover a wide range of fluorescence lines accessible in DAC experiments. At lower energies, absorption of fluorescence X-rays by the diamond and the air between detector and DAC becomes dominant. At higher energies, the efficiency of the polycapillary deteriorates owing to the critical angle for total reflection and the significant transmission of the hard X-rays through the capillary material. Additionally, the capillary was designed to cover the solid angle predetermined by fluorescence acquisition in 90° geometry for the DACs used here. Design and manufacturing of the polycapillary were by XOS (East Greenbush, NY, USA). The detector polycapillary tube has a length of 65 mm and a diameter of 12 mm. The optical input diameter is 4.85 mm and the output diameter 7.57 mm. Entrance and exit are covered by a Be foil of thickness 12.7 µm. Transmission of the polycapillary is 23.4% at 17.4 keV and 46.7% at 8 keV as measured by the manufacturer using X-ray tube sources. The polycapillary was characterized further by knife-edge scans of thin Au and Nb foils using the synchrotron radiation beam at beamline L, HASYLAB.

The polycapillary is mounted on the nozzle of the fluorescence detector using an adapter made of aluminium (Fig. 1). The position of the detector with the mounted polycapillary has to be aligned to the focal spot of the incoming beam. This alignment is achieved using the signal of a thin metal foil positioned in the focal spot of the incoming beam. The foil is oriented at 45° to the beam to permit acquisition of the fluorescence signal at 90°. The position of the detector capillary is optimized by scans of the detector position in the vertical direction and in the direction parallel to the beam. The nominal distance of 50 mm between capillary and focal spot was verified by measuring the focal spot with the distance set to values below and above this nominal distance. At each distance the size of the probed spot is determined by scanning a thin metal foil through the probing volume defined by the focus of the beam and the detector capillary (see also Schmitz *et al.*, 2009). The scan is performed in the direction perpendicular to the foil surface, *i.e.* at 45° to the incoming beam. Such scans were also used to characterize the spatial resolution of the confocal set-up. For these tests, Cu and Nb foils were used to measure the effect of fluorescence energy on the spatial resolution.

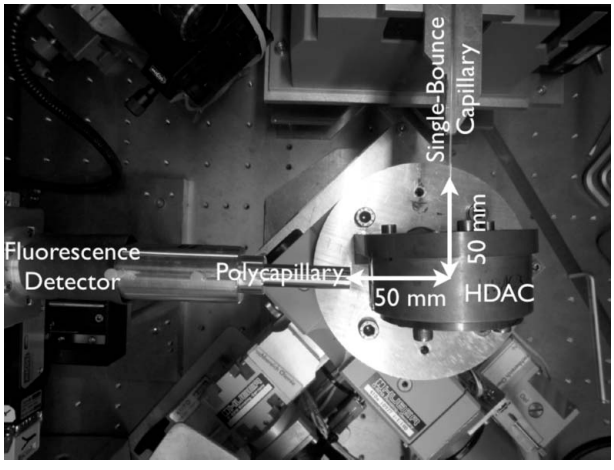

Figure 1
Photograph showing the top view of the experimental set-up at beamline L. The hydrothermal diamond-anvil cell (HDAC) is mounted on a motorized *XYZ* sample stage and can be rotated around the vertical axis. The confocal probing volume defined by the single-bounce capillary and the detector capillary is positioned at the centre of the cell.

2.2. Beamlines

The set-up was tested at two beamlines: beamline L, HASYLAB, and ID24, ESRF. Beamline L uses synchrotron radiation from a bending magnet at the DORIS III storage ring that is run with positrons at an energy of 4.5 GeV and 80–140 mA ring current. A large-bandwidth multilayer monochromator was used to achieve a monochromatic beam with high photon flux. The multilayer monochromator consists of a Ni/C structure. The monochromator was adjusted to an excitation energy of 20 keV. The beam was focused using a single-bounce capillary that allows focusing of X-rays up to 40 keV down to a spot size of ~10 µm (Falkenberg *et al.*, 2003; Schmidt *et al.*, 2007) with a focal distance of 50 mm (see also Fig. 1). An ionization chamber filled with air was used to measure the intensity of the incoming beam. The fluorescence was recorded using an energy-dispersive Vortex Si drift-chamber solid-state detector.

Beamline ID24 is located at an undulator source of the ESRF, where the storage ring is run with electrons at an energy of 6 GeV and 200 mA ring current. The optical layout at ID24 is designed for dispersive X-ray absorption spectroscopy (XAFS) (Pascarelli *et al.*, 2006). In the so-called TURBO-XAS mode, XAFS spectra can be acquired using the fluorescence yield for samples with low concentrations of the element of interest (Pascarelli *et al.*, 1999). In this mode a narrow slit is scanned through the energy-dispersed radiation fan downstream of the polychromator to record the fluorescence yield as a function of the X-ray energy. For the experiment here, we used a Si(111) Bragg polychromator to achieve the energy resolution necessary to perform XAFS measurements. The optical layout consists of two Si mirrors in a Kirkpatrick–Baez configuration, followed by the crystal polychromator and by a third vertically refocusing mirror positioned just before the sample. Further details of the optical layout are reported by Pascarelli *et al.* (2006). The diameter of the spot was 7 µm FWHM at ~10 keV. The

intensity of the incoming beam was measured with a Si photodiode located between the last mirror and the DAC, with the diode recording radiation scattered from a Kapton foil. The fluorescence was recorded using an energy-dispersive Vortex Si drift-chamber solid-state detector (see also Stechern *et al.*, 2009).

2.3. Hydrothermal diamond-anvil cell

A hydrothermal diamond-anvil cell (HDAC) optimized for XRF measurements was used for the experiments (Schmidt & Rickers, 2003; Schmidt *et al.*, 2007; Borchert *et al.*, 2009). A sketch of the HDAC is shown in Fig. 2. The sample chamber of the cell consists of a cylindrical hole in a polished Re or Ir gasket and a recess in the culet face of one diamond anvil. The gasket seals the sample chamber and separates the two diamond anvils. The gaskets used here had an initial diameter of $\sim$500 µm and a thickness of 120 µm. The recess in the diamond anvil has a diameter of 200 µm and a depth of 60 to 80 µm. The recess allows acquisition of the fluorescence signal at an angle of 90° to the incident beam, which minimizes the background by scattered radiation. Additionally, the recess represents most of the sample volume from which fluorescence X-rays are collected. The solid angle accessible for fluorescence detection is about 0.2 × 0.3 rad, and is defined by the gasket, an opening in the cement with which the diamonds are mounted, and the window in the cover ring of the cell. The HDAC is heated by NiCr coils around the tungsten carbide seats. Two K-type thermocouples attached to the diamonds were used to measure the temperature. At room temperature the assemblage in the sample chamber consisted of solid starting materials, an aqueous liquid (*e.g.* H_2O or NaCl–H_2O solution) and a vapour bubble. The actual electrolyte concentration of the solution in the sample chamber was obtained from cryometry, *i.e.* measurement of the vapour-saturated liquidus temperature. The density of the fluid was determined from the temperature of vapour–liquid homogenization. The pressure at a given temperature, concentration and density was calculated using appropriate equations of state or correlation functions (Schmidt & Rickers, 2003, 2007; Borchert *et al.*, 2009). The sample chamber was monitored optically using a microscope to record all phase transitions and sample changes that occur during freezing, heating, annealing and quenching. Element concentrations in the aqueous fluid at pressure and temperature were determined by scaling the fluorescence peak net intensity of an unknown with the net intensity collected for this element on a standard solution in the sample chamber of the cell. Spectra of standard solution and unknown were acquired with the same excitation conditions and geometrical set-up and both net intensities are normalized to the density of each solution. This direct calculation of the concentration in the unknown is valid if the concentrations of major components in both sample and standard solution are similar (*e.g.* Schmidt & Rickers, 2003; Schmidt *et al.*, 2007). If the solution composition for the unknown differs significantly from that of the standard solution, a correction was applied for the absorption of the fluorescence along the path through the fluid in the recess (see also Manning *et al.*, 2008).

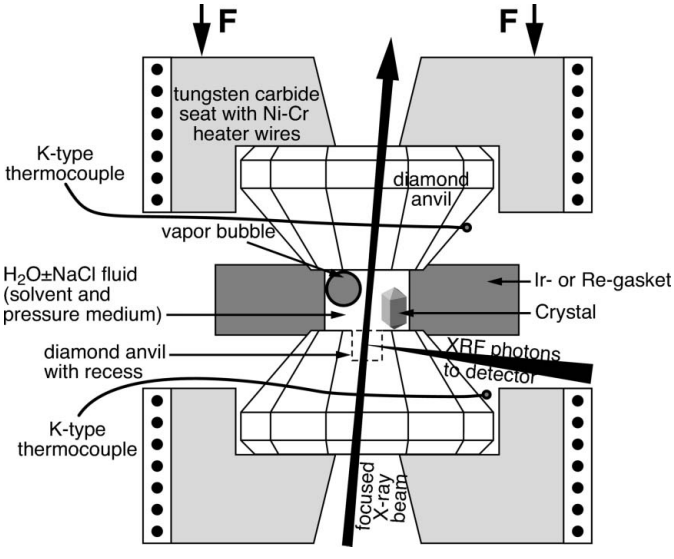

Figure 2
Schematic drawing showing the details of the hydrothermal diamond-anvil cell designed for the *in situ* analysis of fluids at high pressures and temperatures using XRF analysis. Modified after Schmidt *et al.* (2007).

3. Results and discussion

The detector polycapillary was tested at beamline L, HASYLAB, with an incident beam energy of 20 keV. At this energy the transmission of the polycapillary was 19.1% using a horizontal beam dimension of 3 mm and a vertical dimension of 1.5 mm at the entrance slit. This result is consistent with the values determined by the manufacturer at 17.4 keV (23.4%), because the transmission decreases with increasing X-ray energy. An edge scan on a Nb foil with a thickness of 2.5 µm revealed a beam size of 148 µm (FWHM) at 20 keV. This measured value agrees well with the design parameters given by the manufacturer ($\leq$160 µm at 17.4 keV and $\leq$300 µm at 8.0 keV), which are based on simulation data. A gain factor of 50 at 16.6 keV was obtained from comparison of the flux through the entrance slit (1.5 mm × 3 mm) with that transmitted through the polycapillary.

The spatial resolution defined by the aligned capillaries in the incoming beam and in front of the detector was measured by scanning the probing volume with thin metal foils. Fig. 3 shows the fluorescence intensity as a function of the stage position of one scan using an 8 µm-thick Cu foil and one scan on a 2.5 µm-thick Nb foil. Both scans were performed at beamline L, HASYLAB. The FWHM of the peaks are 225 µm in the case of the Cu foil (8 keV) and 108 µm for the Nb foil (16.6 keV). The FWHM of the measured profiles can be related to the probing volume and the thickness d of the foil (Janssens *et al.*, 2004),

$$\mathrm{FWHM}^2_{\mathrm{profile}} = \mathrm{FWHM}^2_{\mathrm{SBC}} + \mathrm{FWHM}^2_{\mathrm{DPC}} + d^2_{\mathrm{foil}}, \qquad (1)$$

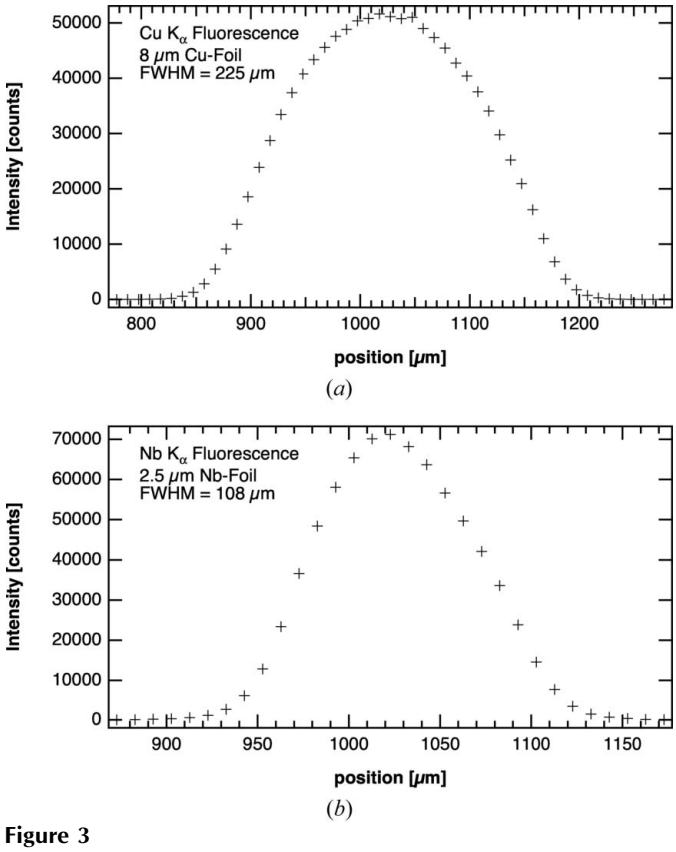

Figure 3
Fluorescence intensity *versus* stage position for scans of a thin Cu foil (*a*) and a thin Nb foil (*b*) through the probing volume as indicated. Full width at half-maximum (FWHM) values given were determined from the data.

where $\mathrm{FWHM}^2_{\mathrm{SBC}} + \mathrm{FWHM}^2_{\mathrm{DPC}}$ describes the width of the probing volume defined by the single-bounce capillary and the detector polycapillary. Using this equation and the known values for the single-bounce capillary and the foil thickness, the width of the focal spot of the detector polycapillary was calculated from the measured profiles. This resulted in the same values as those determined directly on the profiles, *i.e.* 108 µm and 225 µm. Thus, in this type of scan, which characterizes the depth of the probing volume in the direction 45° to the incoming beam, the detector capillary governs the width of the profile.

Additional information on the spatial resolution at the conditions of *in situ* experiments is provided by scans across HDAC sample chambers that contained zircon ($ZrSiO_4$) or hafnon ($HfSiO_4$) crystals. Such a sample chamber is shown in Fig. 4(*a*) with a zircon crystal located at the lower rim of the gasket and aqueous solution, in which a portion of the zircon had dissolved. For this measurement the cell was rotated by 3° around the vertical axis with respect to the beam, which maximizes the solid angle for the fluorescence in the direction of the detector and avoids reduction of the signal by absorption in the gasket. In a vertical scan across this chamber (Fig. 4*b*) the Zr K_α signal from the solution in the recess can be well separated from that from the zircon crystal. Therefore, the position of the crystal in the sample chamber relative to the recess is not as crucial as in experiments without detector capillary, where care must be taken that the signal from the solution in the recess is not superimposed by signal from co-excitation of the crystal by scattered X-rays of the incident beam. For example, in the study of Schmidt & Rickers (2003) the crystal was placed in an extra pocket drilled into the rim of the gasket to avoid co-excitation. Fig. 4(*c*) shows a similar example, where the cell was not rotated, *i.e.* in line with the axis of the beam. In this case the vertical scan across the chamber (Fig. 4*d*) shows only the Zr K_α signal from the recess, whereas fluorescence from the zircon crystal is not visible at all. In this orientation of the cell the confocal set-up thus allows a complete suppression of the signal by the crystal at any location in the gasket hole. In Fig. 4(*e*) an example is shown where a hafnon crystal has shifted closer to the recess during the run and a second Hf-bearing crystal has grown at the lower rim of the recess. In the first scan of the Hf L_α intensity across the sample chamber the hafnon crystal at the margin of the sample chamber is clearly visible from the sharp increase in intensity. However, this signal does not affect the intensity representative of the Hf concentration in the fluid measured in the recess. The second scan shows that the crystal shifted towards the recess and that a second Hf-bearing crystal grew at the rim of the recess. However, the transition of the signal from the crystal to the remaining recess is still very sharp. More importantly, the Hf L_α intensity in the remaining portion of the recess is very close to that in the first scan. Both scans indicate that determined Hf concentrations for the fluid based on the measured L_α intensity in the recess are not affected by co-excitation of the solid Hf phases even under this unfavourable geometric arrangement of crystal and recess.

Fig. 5(*a*) compares XRF spectra measured at beamline L, HASYLAB, on a 1300 p.p.m. Zr standard solution in the sample chamber of a HDAC. One spectrum was acquired using the confocal set-up with the detector capillary, whereas the other was measured using a collimator on the fluorescence detector with 2 mm diameter at a distance of 50 mm from the centre of the HDAC. First of all, the total signal recorded by the detector when using the detector capillary is drastically decreased. This decrease is due to a smaller solid angle seen by the detector, the transmission of the polycapillary, which is smaller than 100%, and higher absorption because of the longer distance between probing volume and detector. For Zr K_α the intensity is reduced by a factor of 3.4 for the spectrum acquired with the capillary. However, the ratio between the Zr K_α peak maximum and the maximum of the Compton scattering increases from 0.5 in the spectrum recorded with the collimator to 1.3 if the detector capillary was used. Inspection of the spectrum acquired with the collimator indicates that the influence of the Compton scattering on the measured signal extends down to about 14 keV at an excitation energy of 20 keV. The spectrum acquired with the detector polycapillary indicates a much lower intensity of the scattered radiation (by a factor of ten). The contribution to the signal becomes already negligible between 15 and 16 keV. The strong signal from elastic and inelastic scattering is produced along the path of the incident beam through the diamond anvil. The detector polycapillary efficiently suppresses collection of this signal. In addition, the intensity of Re

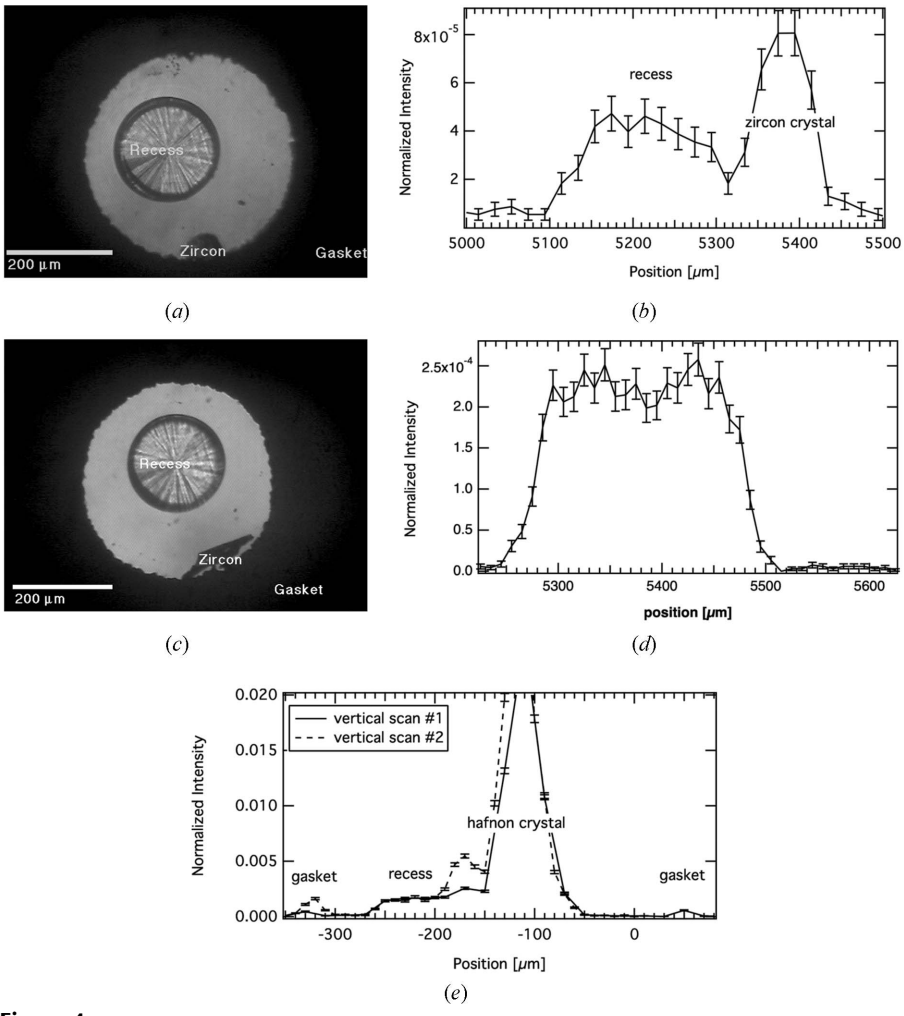

Figure 4
(*a*) Photograph of the sample chamber of the HDAC containing a zircon crystal ($ZrSiO_4$) and an aqueous solution at 1023 K. (*b*) Vertical scan of Zr K_α intensity normalized to the incident beam intensity across the sample chamber shown in (*a*). Error bars indicate the standard deviation of the measured signal. Measurement was performed at beamline L. (*c*) Photograph of the sample chamber of the HDAC containing a zircon crystal ($ZrSiO_4$) and an aqueous solution at 873 K. (*d*) Vertical scan of Zr K_α intensity normalized to the incident beam intensity across the sample chamber shown in (*c*). Error bars indicate the standard deviation of the measured signal. The measurement was performed at beamline L. (*e*) Vertical scans of the Hf L_α intensity normalized to the incident beam intensity across the sample chamber containing a hafnon crystal ($HfSiO_4$) at various positions to the recess. See text for details. Scans show two points in time. Error bars indicate the standard deviation of the measured signal. Measurements were performed at ID24.

fluorescence lines from the gasket is decreased by a factor of 12. Finally, the spectrum collected with the collimator shows a Sr K_α peak at 14.2 keV, which is not present in the other spectrum and thus indicates a contribution generated outside the sample chamber.

The spectra shown in Fig. 5(*b*) were taken on a 1000 p.p.m. Hf standard solution and on a NaOH solution which contained ~400 p.p.m. Hf due to equilibration with a hafnon crystal at 673 K. Both spectra were acquired at ID24, ESRF. Fluorescence peaks of Fe, Ni and Zn are present in addition to the *L* lines of Hf. The intensities of the Fe, Ni and Zn lines correlate with those of the Hf lines. The exact source for these lines could not be determined, but they are probably generated by secondary excitation of these elements along the path of the fluorescence and the scattered radiation to the detector.

Detection limits (DLs) for this set-up were estimated based on the spectra measured on several standard solutions from the relationship

$$\mathrm{DL} = C_{\mathrm{STD}}\, 3\,(I_{\mathrm{BC}})^{1/2}/I_{\mathrm{Peak}}, \qquad (2)$$

where C_{STD} denotes the concentration of the standard solution, I_{BC} the intensity of the background and I_{Peak} the intensity of the fluorescence peak (*e.g.* Haller & Knöchel, 1996). Peak and background intensities were determined using the software package *AXIL* (*e.g.* Vekemans *et al.*, 1995). Using the K_α peak, a relative DL of 1 p.p.m. was obtained for Zr (500 s acquisition time) for the set-up with detector polycapillary at beamline L. This value is similar or even slightly better than that obtained with the classical set-up. The DLs for the classical set-up range between 1 and 3 p.p.m., including earlier measurements of Schmidt *et al.* (2006) for the HDAC set-up at beamline L (1000 s acquisition time). At the used excitation conditions the fluorescence spectra taken at ID24 yield a DL for Hf of 0.5 p.p.m. based only on the L_α peak (500 s acquisition time). Both cases show that the confocal set-up leads to sensitivities that are similar or even better than those obtained with the classical set-up. Enhancement of the DL certainly stems from the improved peak-to-background ratio. However, the enhancement is limited by two other factors: (i) the transmission of the polycapillary is smaller than 100% (see §2); (ii) the distance between the detector and probing volume is significantly longer, so that absorption reduces the fluorescence intensity particularly at lower energies (*e.g.* in the case of Hf). The enhancement of DL that was observed here is consistent with earlier results by Janssens *et al.* (2004) for the confocal set-up, who report improvements especially for thick samples, where background from inelastic scattering is more severe.

Finally, the confocal set-up was also applied at ID24 to record fluorescence XAFS spectra at the Hf *L*-edge on aqueous solutions at high temperature and pressure. Two examples are shown in Fig. 6, which illustrate the potential for acquisition of XANES or EXAFS spectra at the given concentrations. At a solute concentration of ~400 p.p.m. Hf the signal was weak, so that it was only worthwhile acquiring an extended XANES range, with 40 s point^{-1} At 5000 p.p.m. Hf, acquisition of EXAFS spectra became feasible, as demonstrated by the spectrum of Hf in the $Na_2Si_3O_7$-bearing

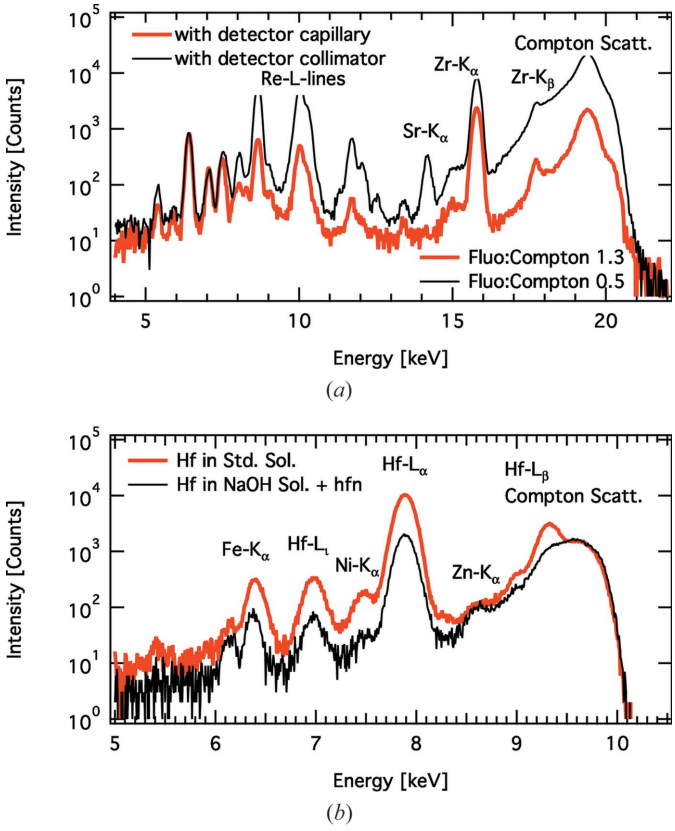

Figure 5
(*a*) X-ray fluorescence spectra of a standard solution containing 1300 p.p.m. Zr loaded into the HDAC. The spectra were measured at beamline L with the detector capillary or detector collimator as indicated. (*b*) X-ray fluorescence spectra of a standard solution containing 1000 p.p.m. Hf loaded into the HDAC measured at room temperature and of a NaOH solution (35 wt%) equilibrated with a hafnon crystal at 773 K (∼400 p.p.m. Hf). The spectra were measured at ID24 using the detector capillary.

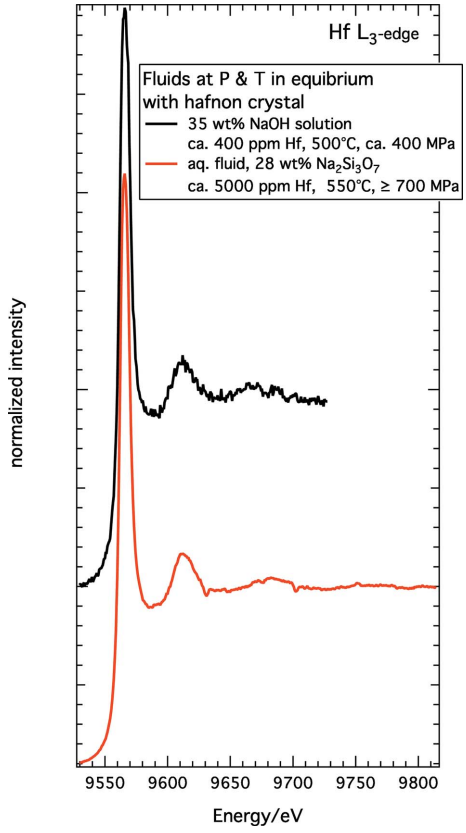

Figure 6
Fluorescence XAFS spectra taken at ID24 on solutions in the HDAC at the conditions indicated.

aqueous solution, collected with 50 s point^{-1}. The spectrum corresponds to an EXAFS range of 8 Å^{-1}. It is noted here that all XAFS spectra collected in this study showed very little distortions in the raw data, *i.e.* fluorescence yield normalized to the intensity of the incoming beam. This does not only indicate an appropriate set-up for measurement of the intensity of the incoming beam but also that the confocal set-up reduces contributions from scattered radiation to the background of the fluorescence lines of interest (here Hf). Usually, such a background contribution is excitation-energy-dependent because of the increasing difference between fluorescence and excitation energy, which changes the background and leads to tilting or distortion of the XAFS spectrum.

4. Conclusion and outlook

The results shown here demonstrate the advantages of a confocal micro-XRF set-up for experiments with diamond-anvil cells. This set-up enhances the quality of the fluorescence spectra, and thus the sensitivity for detecting elements at low concentrations. The confocal X-ray optical set-up significantly facilitates HDAC experiments, particularly those involving the dissolution of substances in fluids. This is because it efficiently suppresses unwanted fluorescence signal from inside and outside the sample chamber of the DAC as well as contributions by elastically and inelastically scattered radiation of the incoming beam formed on the path through the diamond anvil. Specifically, the actual location of a mineral relative to the recess in the sample chamber of the HDAC is less crucial for confocal spectrum acquisition because it is easier to avoid collection of XRF from co-excitation of the mineral by scattered X-rays in the upstream diamond anvil. The examples shown were acquired with detection at 90° to the incoming synchrotron radiation beam. However, most DACs do not allow the detection of the fluorescence signal at this angle, or only if a Be gasket is used, which is transparent to X-rays but poses many other experimental limitations. Sanchez-Valle *et al.* (2003) used a membrane-driven DAC and a position of the fluorescence detector at 15° to the incoming beam. In this forward-scattering geometry, however, the signal from Compton scattering becomes huge. A confocal set-up similar to the one proposed here should provide an efficient means of reducing this signal, and would thus greatly enhance the sensitivity of XRF analyses in forward-scattering DAC experiments.

We thank M. Kreplin, R. Schulz, the staff of the high-pressure workshop at GFZ, W. Ternes at DESY as well as

F. Perrin at ESRF for technical help and support. Financial support by the DFG through the grant Wi 2000/5-1 and by the GFZ through W. Heinrich is highly appreciated. HASYLAB at DESY and the ESRF are thanked for granting beam time.

References

Boehler, R. (2005). *EMU Notes Mineral.* **7**, 217–224.
Borchert, M., Wilke, M., Schmidt, C. & Rickers, K. (2009). *Chem. Geol.* **259**, 39–47.
Falkenberg, G., Rickers, K., Bilderback, D. H. & Huang, R. (2003). *HASYLAB Annual Report*, pp. 71–74. HASYLAB, Hamburg, Germany.
Haller, M. & Knöchel, A. (1996). *J. Trace Mircroprobe Tech.* **14**, 461–488.
Janssens, K., Proost, K. & Falkenberg, G. (2004). *Spectrochim. Acta B*, **59**, 1637–1645.
Kanngiesser, B., Malzer, W. & Reiche, I. (2003). *Nucl. Instrum. Methods Phys. Res. B*, **211**, 259–264.
Keppler, H. & Frost, D. J. (2005). *EMU Notes Mineral.* **7**, 1–30.
Manning, C. E., Wilke, M., Schmidt, C. & Cauzid, J. (2008). *Earth Planet. Sci. Lett.* **272**, 730–737.
Mayanovic, R., Anderson, A. J., Bassett, W. A. & Chou, I. M. (2007). *Rev. Sci. Instrum.* **78**, 053904.
Pascarelli, S., Mathon, O., Muñoz, M., Mairs, T. & Susini, J. (2006). *J. Synchrotron Rad.* **13**, 351–358.
Pascarelli, S., Neisius, T. & De Panfilis, S. (1999). *J. Synchrotron Rad.* **6**, 1044–1050.
Sanchez-Valle, C., Daniel, I., Martinez, I., Simionovici, A. & Reynard, B. (2004). *J. Phys. Condens. Matter*, **16**, S1197–S1206.
Sanchez-Valle, C., Martinez, I., Daniel, I., Philippot, P., Bohic, S. & Simionovici, A. (2003). *Am. Mineral.* **88**, 978–985.
Schmidt, C. & Rickers, K. (2003). *Am. Mineral.* **88**, 288–292.
Schmidt, C., Rickers, K., Bilderback, D. H. & Huang, R. (2007). *Lithos*, **95**, 87–102.
Schmidt, C., Rickers, K., Wirth, R., Nasdala, L. & Hanchar, J. (2006). *Am. Mineral.* **91**, 1211–1215.
Schmitz, S., Möller, A., Wilke, M., Malzer, W., Kanngiesser, B., Bousquet, R., Berger, A. & Schefer, S. (2009). *Eur. J. Mineral.* **21**, 927–945.
Stechern, A., Wilke, M., Schmidt, C., Rickers, K., Pascarelli, S. & Manning, C. E. (2009). *J. Phys. Conf. Ser.* **190**, 012058.
Vekemans, B., Janssens, K., Vincze, L., Adams, F. & Van Espen, P. (1995). *Spectrochim. Acta B*, **50**, 149–169.
Vincze, L., Vekemans, B., Brenker, F. E., Falkenberg, G., Rickers, K., Somogyi, A., Kersten, M. & Adams, F. (2004). *Anal. Chem.* **76**, 6786–6791.
Wilke, M., Schmidt, C., Farges, F., Malavergne, V., Gautron, L., Simionovici, A., Hahn, M. & Petit, P. E. (2006). *Chem. Geol.* **229**, 144–161.